Effect of an Armature Winding Misalignment on Passively Levitated Self-Bearing Machines

Joachim Van Verdeghem, Bruno Dehez
Institute of Mechanics, Materials and Civil Engineering (IMMC)
Université catholique de Louvain (UCLouvain)
Louvain-La-Neuve, Belgium
joachim.vanverdeghem@uclouvain.be

***Abstract*—Passively levitated self-bearing machines provide the rotor drive and guidance within a single structure without requiring controllers, power electronics and sensors dedicated to the magnetic suspension, leading to compact, reliable and cost-effective systems. Electromechanical models describing their rotor dynamics have recently been derived and experimentally validated. However, these models do not account for non-idealities that could arise from manufacturing imperfections. In this context, this paper investigates the impact of an angular misalignment between the upper and lower windings of passively levitated self-bearing machines on the force and torque production. The existing electromechanical model is extended, highlighting that this misalignment slightly degrades the driving torque and the conventional passive restoring force, on the one hand, and creates additional force and torque components, on the other hand. Among the latter, those arising from the suspension currents are independent from the rotor axial displacement and are thus produced even in centred position, thereby potentially acting as disturbances. Finally, an experimental study is carried out, allowing to validate the suspension force produced by the machine in quasi-static conditions and to confirm the interest of accounting for this winding non-ideality in the model.**

***Index Terms*—Bearingless machines, Self-bearing motors, Passive suspension, Angular misalignment, Electromechanical model**

I. Introduction

Self-bearing machines have been developed for high-speed and high-torque density systems by integrating the rotor drive and guidance within a single structure, thereby taking advantage of magnetic suspension benefits, such as the elimination of mechanical friction, wear and lubrication [1]. Their applications thus encompass blower and fans [2], pumps [3–5], compressors [6], flywheels [7–9] and reaction wheels [10].

The rotor magnetic suspension is typically achieved by actively controlling the currents flowing through the machine windings, either dedicated to the levitation or shared with the drive [11–13], based on the position measurement. Although this approach can be applied to all five rotor degrees of freedom [14, 15], self-bearing machines often integrate passive suspension mechanisms to support the shaft along one or more of these axes. In slice motors, reluctance forces provide passive stabilisation in the axial and tilt directions whereas the radial degrees of freedom are actively regulated [16–18]. In single-drive machines, permanent magnet bearings generally ensure the rotor radial and tilt levitation, thereby limiting the requirement for active control to the axial position [19–21].

Passively levitated self-bearing machines, that rely on the operation principle of electrodynamic suspensions, stand out thanks to the absence of controllers, power electronics and sensors dedicated to the rotor magnetic levitation, resulting in more compact, reliable and cost-effective systems. By circumventing Earnshaw's theorem, these machines can be combined with centring permanent magnet bearings to implement fully passive magnetic suspension. Electromechanical models have been established to predict the rotor axial and rotational dynamics based on the global parameters of the machine [22–24] and have been experimentally validated, both for axial-flux [25, 26] and radial-flux structures [27–29]. However, these models have not considered non-idealities caused by manufacturing imperfections so far, assuming that a proper commissioning phase can mitigate them, while this may not be feasible in mass production.

In this context, this paper studies the impact of an angular misalignment between the upper and lower windings on the force and torque capabilities. The existing electromechanical model is generalised to account for this non-ideality and validated through experimental measurements.

The paper is structured as follows. Section II describes the machine structure and operation principle. The electromechanical model considering the winding angular misalignment is then established in Section III. Following on from this, the experimental setup, including the prototype and test stand, is presented in Section IV. Finally, the experimental validation of the proposed model is carried out in Section V.

II. Machine Description

This section first describes the structure of the self-bearing machine, including the winding non-ideality being investigated, and then outlines its operation principle.

A. Structure

The machine can be implemented based on either an axial-flux or a radial-flux structure, as depicted in Fig. 1(a) and 1(b) respectively. In both cases, the rotor consists of a permanent

The present research is part of the Space4ReLaunch project, which is supported by the SPW Economie Emploi Recherche of the Walloon Region, under the grant agreement #2210181.

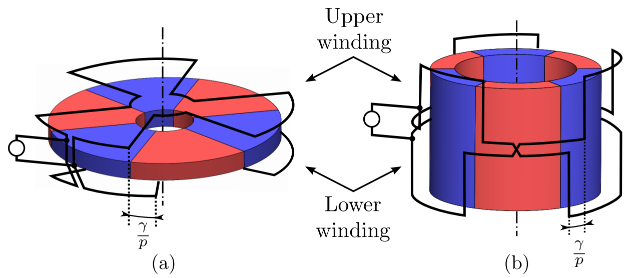

Fig. 1: Self-bearing machine (only one phase represented and with $p=3$). (a) Axial-flux structure. (b) Radial-flux structure.

magnet arrangement producing a p pole-pair magnetic field that interacts with an ironless armature composed of two three-phase windings connected in parallel to the power supply. These windings, referred to as the upper and lower ones, may be angularly misaligned by a mechanical angle γ/p due to manufacturing inaccuracies.

B. Operation Principle

The self-bearing machine under study provides both the rotor drive and passive axial suspension.

In centred axial position, i.e. $z=0$, the permanent magnet fluxes linked by the upper and lower windings are identical and so are the resulting electromotive forces. Consequently, the current supplied by the three-phase voltage source distributes equally between the two windings connected in parallel, only producing a drive torque $T_{\alpha,M}$ as in a conventional motor.

In case of rotor axial displacement, namely $z \neq 0$, the imbalance between the upper and lower flux linkages leads to an uneven distribution of currents between both windings. As discussed in [22], the upper and lower currents, denoted $\mathbf{i_U}$ and $\mathbf{i_L}$, can be seen as the superposition of the motor currents $\mathbf{i_M}$ and the suspension currents $\mathbf{i_S}$, defined as follows:

$$\begin{aligned}\mathbf{i_M} &= \mathbf{i_U} + \mathbf{i_L}\\ \mathbf{i_S} &= \frac{\mathbf{i_U} - \mathbf{i_L}}{\mathbf{2}}\end{aligned} \tag{1}$$

The former relate to the currents provided by the power supply and still solely generate the drive torque $T_{\alpha,M}$. In contrast, the latter correspond to circulating currents flowing through the closed loop constituted of both windings that are short-circuited on each other and create a passive axial force $F_{z,S}$, that tends to restore the rotor towards its centred position, and a drag torque $T_{\alpha,S}$, that opposes to the rotation.

III. Electromechanical Model

This section extends the electromechanical model derived in [22] by taking into account a misalignment between the upper and lower windings. To that end, the permanent magnet flux linkages are first established and substituted into the governing electrical equations. The electromagnetic forces are then developed and finally analysed in quasi-static conditions.

A. PM Flux Linkages

The angular misalignment γ/p between the upper and lower windings induces a phase shift γ between the permanent magnet fluxes linked by these latter, denoted $\mathbf{\Phi_U}$ and $\mathbf{\Phi_L}$ respectively. Assuming small rotor axial displacements z and considering only the fundamental frequency of the magnetic field, these flux linkages can be expressed as:

$$\begin{aligned}\mathbf{\Phi_U} &= (K_\alpha + zK_z)\cos\left(p\alpha - \boldsymbol{\delta} - \frac{\gamma}{2}\right)\\ \mathbf{\Phi_L} &= (K_\alpha - zK_z)\cos\left(p\alpha - \boldsymbol{\delta} + \frac{\gamma}{2}\right)\end{aligned}, \tag{2}$$

where α is the rotational position of the rotor, K_α is the flux constant, corresponding to the flux amplitude when the rotor is in axial centred position ($z=0$), K_z is the flux gradient, namely the proportionality coefficient between the flux amplitude and the axial displacement z, and $\boldsymbol{\delta} = [0,\ 2\pi/3,\ 4\pi/3]$ includes the angular position of the three phase windings.

As presented in [22], the motor and suspension flux linkages, referred to as $\mathbf{\Phi_M}$ and $\mathbf{\Phi_S}$ respectively, can be defined based on the upper and lower ones:

$$\begin{aligned}\mathbf{\Phi_M} &= \frac{\mathbf{\Phi_U} + \mathbf{\Phi_L}}{2}\\ &= K_\alpha \cos\left(\frac{\gamma}{2}\right)\cos\left(p\alpha - \boldsymbol{\delta}\right)\\ &\quad + zK_z\ \sin\left(\frac{\gamma}{2}\right)\sin\left(p\alpha - \boldsymbol{\delta}\right)\\ \mathbf{\Phi_S} &= \mathbf{\Phi_U} - \mathbf{\Phi_L}\\ &= 2\ zK_z \cos\left(\frac{\gamma}{2}\right)\cos\left(p\alpha - \boldsymbol{\delta}\right)\\ &\quad + 2\ K_\alpha \sin\left(\frac{\gamma}{2}\right)\sin\left(p\alpha - \boldsymbol{\delta}\right)\end{aligned}. \tag{3}$$

The former represent the fluxes seen from the power supply terminals whereas the latter correspond to those intercepted by the short-circuited paths consisting of the upper and lower windings. In both expressions, the presence of an angular misalignment γ introduces an additional flux component that is in quadrature with respect to that without non-ideality. Regarding the motor fluxes $\mathbf{\Phi_M}$, the additional component evolves linearly with the rotor axial displacement z and thus cancels out in nominal position. In contrast, as far as the suspension fluxes $\mathbf{\Phi_S}$ is concerned, it is independent from the rotor excursion z, unlike the ideal case component. Consequently, this manufacturing imperfection of the armature winding prevents the self-bearing machine from satisfying the null-flux principle, resulting in currents and thus losses even when the rotor is centred, as confirmed in Section III-D.

B. Electrical Equations

Assuming that the inductance coefficients are independent from the rotor axial and rotational positions, Faraday's law applied to the upper and lower windings of each phase yields:

$$\begin{aligned}\mathbf{u} &= R\mathbf{i_U} + \mathbf{L}\frac{d\mathbf{i_U}}{dt} + \mathbf{M}\frac{d\mathbf{i_L}}{dt} + \frac{d\mathbf{\Phi_U}}{dt}\\ \mathbf{u} &= R\mathbf{i_L} + \mathbf{L}\frac{d\mathbf{i_L}}{dt} + \mathbf{M}\frac{d\mathbf{i_U}}{dt} + \frac{d\mathbf{\Phi_L}}{dt}\end{aligned} \tag{4}$$

where R is the electrical resistance, $\mathbf{u}$ is the three-phase voltage applied on the armature, $\mathbf{L}$ includes the self and mutual inductance coefficients of the upper/lower windings, and $\mathbf{M}$ contains the mutual inductance coefficients between the upper and lower windings:

Substituting (1) and (3) into (4) allows us to emphasize the electrical equations governing the motor and suspension functions of the self-bearing machine:

$$\begin{aligned} \mathbf{u} &= \frac{R}{2}\ \mathbf{i_M} + \left(\frac{\mathbf{L}+\mathbf{M}}{2}\right)\frac{d\mathbf{i_M}}{dt} + \frac{d\mathbf{\Phi_M}}{dt} \\ 0 &= 2R\ \mathbf{i_S} + 2\left(\mathbf{L}-\mathbf{M}\right)\frac{d\mathbf{i_S}}{dt} + \frac{d\mathbf{\Phi_S}}{dt} \end{aligned} . \tag{5}$$

The motor currents $\mathbf{i_M}$ are supplied by the voltage source $\mathbf{u}$ and flow through both windings connected in parallel whereas the suspension currents $\mathbf{i_S}$ are passively induced within a closed path formed by the series connection of these windings due to the electromotive force terms and therefore circulate independently from the power supply $\mathbf{u}$. Interestingly, this highlights that the rotor levitation is still ensured when disconnecting the voltage source from the armature winding.

Applying the Park-Concordia transformation to (5) leads to:

$$\begin{aligned} u_d &= \frac{R}{2}\ i_{M,d} + \frac{L_M}{2}\left(\dot{i_{M,d}} - p\omega i_{M,q}\right) \\ &\quad + \sqrt{\frac{3}{2}}p\omega z K_z \sin\left(\frac{\gamma}{2}\right) \\ u_q &= \frac{R}{2}\ i_{M,q} + \frac{L_M}{2}\left(\dot{i_{M,q}} + p\omega i_{M,d}\right) \\ &\quad + \sqrt{\frac{3}{2}}\left[p\omega K_\alpha \cos\left(\frac{\gamma}{2}\right) - \dot{z}K_z \sin\left(\frac{\gamma}{2}\right)\right] \\ 0 &= 2R\ i_{S,d} + 2L_S\left(\dot{i_{S,d}} - p\omega i_{S,q}\right) \\ &\quad + \sqrt{6}\left[\dot{z}K_z \cos\left(\frac{\gamma}{2}\right) + p\omega K_\alpha \sin\left(\frac{\gamma}{2}\right)\right] \\ 0 &= 2R\ i_{S,q} + 2L_S\left(\dot{i_{S,q}} + p\omega i_{S,d}\right) \\ &\quad + \sqrt{6}p\omega z K_z \cos\left(\frac{\gamma}{2}\right) \end{aligned} \tag{6}$$

where L_M and L_S are the motor and suspension synchronous inductance coefficients of an upper/lower winding [30]. The first two equations, that govern the evolution of the direct and quadrature axis motor currents, include an additional electromotive force term caused by the winding angular misalignment γ. The latter are proportional to the rotor axial displacement z and speed $\dot{z}$ respectively. This non-ideality therefore creates a coupling between the rotor drive and suspension whenever the rotor deviates from its nominal position.

C. Electromagnetic Model

The electromagnetic model is established based on the magnetic coenergy approach. Assuming the independence of the inductance coefficients from the rotor position and given the ironless stator structure, the force and torque reduce to their electrodynamic contribution, that results from the interaction between the upper and lower PM flux linkages with the currents flowing within the corresponding windings.

1) Axial Force: The total axial force F_z exerted by the self-bearing machine can be calculated as:

$$F_z = \left[\frac{d\mathbf{\Phi_U}}{dz}\right]^{\mathrm{T}}\mathbf{i_U} + \left[\frac{d\mathbf{\Phi_L}}{dz}\right]^{\mathrm{T}}\mathbf{i_L} \tag{7}$$

Injecting (1) and (3) into (7) allows to rewrite this force in terms of the motor and suspension currents and fluxes:

$$F_z = \left[\frac{d\mathbf{\Phi_S}}{dz}\right]^{\mathrm{T}}\mathbf{i_S} + \left[\frac{d\mathbf{\Phi_M}}{dz}\right]^{\mathrm{T}}\mathbf{i_M} \tag{8}$$

The axial force can then be expressed in the synchronous $d-q$ frame by applying the Park-Concordia transformation:

$$F_z = \underbrace{\sqrt{6}K_z\cos\left(\frac{\gamma}{2}\right)i_{S,d}}_{F_{z,S}} - \underbrace{\sqrt{\frac{3}{2}}K_z\sin\left(\frac{\gamma}{2}\right)i_{M,q}}_{F_{z,M}} \tag{9}$$

The first force contribution, noted $F_{z,S}$, lies at the basis of the axial stabilisation of the rotor in the self-bearing machine under study, being produced by the direct-axis component of the passively induced suspension current $i_{S,d}$, and is only marginally affected by the winding angular misalignment γ. On the contrary, the second contribution, denoted $F_{z,M}$, is generated due to this non-ideality of the armature winding by the quadrature-axis motor current $i_{M,q}$ and acts as an axial disturbance force whose significance depends on the rotational acceleration and load torque, the latter including the passive electrodynamic drag torque discussed hereinafter.

2) Torques: The total electromagnetic torque T_α can be derived from the currents and flux linkages of the upper and lower windings, and subsequently decomposed into its motor and suspension components, referred to as $T_{\alpha,M}$ and $T_{\alpha,S}$, by substituting (1) and (3):

$$\begin{aligned} T_\alpha &= \left[\frac{d\mathbf{\Phi_U}}{d\alpha}\right]^{\mathrm{T}}\mathbf{i_U} + \left[\frac{d\mathbf{\Phi_L}}{d\alpha}\right]^{\mathrm{T}}\mathbf{i_L} \\ &= \underbrace{\left[\frac{d\mathbf{\Phi_S}}{d\alpha}\right]^{\mathrm{T}}\mathbf{i_S}}_{T_{\alpha,S}} + \underbrace{\left[\frac{d\mathbf{\Phi_M}}{d\alpha}\right]^{\mathrm{T}}\mathbf{i_M}}_{T_{\alpha,M}} \end{aligned} \tag{10}$$

These torques can be further simplified by rewritting them in the synchronous frame as:

$$\begin{aligned} T_{\alpha,M} &= p\sqrt{\frac{3}{2}}\left[K_\alpha\cos\left(\frac{\gamma}{2}\right)i_{M,q} + zK_z\sin\left(\frac{\gamma}{2}\right)i_{M,d}\right] \\ T_{\alpha,S} &= p\sqrt{6}\left[zK_z\cos\left(\frac{\gamma}{2}\right)i_{S,q} + K_\alpha\sin\left(\frac{\gamma}{2}\right)i_{S,d}\right] \end{aligned} \tag{11}$$

In both expressions, the angular misalignment γ slightly reduces the classical torque contribution associated with the quadrature-axis current, on the one hand, and introduces an additional term generated by the direct component, on the other hand. Regarding the motor torque $T_{\alpha,M}$, the additional term is proportional to the rotor axial displacement z and thus disappears in centred position. It should be noted that this term can generally be considered negligible due to its dependence on the variation of the flux zK_z, which is typically an order of magnitude smaller than the motor flux constant K_α, and on the sine of the misalignment γ. In contrast, concerning the parasitic torque $T_{\alpha,S}$ created by the suspension current i_S, the additional term can not be neglected and may even become the dominant contribution at small rotor displacements z.

D. Quasi-static Analysis

The quasi-static analysis is carried out by considering constant rotor axial position z and rotational speed ω. This approach allows to investigate the suspension currents and the resulting electrodynamic forces and torques under steady-state conditions, thereby providing an insight on the passive suspension performance of the self-bearing machine.

1) Suspension Current: The quasi-static direct and quadrature components of the suspension currents, $i_{S,d}$ and $i_{S,q}$, can be determined by setting the derivatives to zero in (6), yielding:

$$\begin{aligned} i_{S,d} &= -\frac{\sqrt{6}zK_z}{2L_s}\cos\left(\frac{\gamma}{2}\right)\frac{\omega^2}{\omega^2+\omega_e^2} \\ &\quad -\frac{\sqrt{6}K_\alpha}{2L_s}\sin\left(\frac{\gamma}{2}\right)\omega_e\frac{\omega}{\omega^2+\omega_e^2} \\ i_{S,q} &= -\frac{\sqrt{6}zK_z}{2L_s}\cos\left(\frac{\gamma}{2}\right)\omega_e\frac{\omega}{\omega^2+\omega_e^2} \\ &\quad +\frac{\sqrt{6}K_\alpha}{2L_s}\sin\left(\frac{\gamma}{2}\right)\frac{\omega^2}{\omega^2+\omega_e^2} \end{aligned} \tag{12}$$

Assuming no angular misalignment between the upper and lower windings ($\gamma = 0$), the direct-axis current $i_{S,d}$ is predominant at high rotational speeds ω, namely well above the speed $\omega_e = \frac{1}{p}\frac{R}{L_S}$ corresponding to the suspension electrical pole. Indeed, the winding impedance is primarily inductive under these conditions, causing the currents to flow nearly in phase with the suspension flux linkages that generate them. Conversely, the armature winding exhibits a resistive behaviour at low rotational speeds, leading the quadrature component $i_{S,q}$ to prevail. The presence of an angular misalignment γ significantly affects the distribution of the suspension current between its direct and quadrature components, both of them presenting an additional term whose evolution with the rotational speed ω is inverted compared to that of the classical term. This results from the appearance of suspension flux linkage contributions that are in quadrature with respect to the permanent magnet flux density, as stated in Section III-A. Importantly, these additional terms are independent from the rotor axial displacement z, implying that currents and losses are generated even in centred position.

2) Suspension Force: The suspension force $F_{z,S}$ exerted by the self-bearing machine in quasi-static conditions can be obtained by substituting (12) into (9):

$$\begin{aligned} F_{z,S} = &- z\underbrace{\frac{3K_z^2}{L_S}\cos^2\left(\frac{\gamma}{2}\right)\frac{\omega^2}{\omega^2+\omega_e^2}}_{k_{z,S}} \\ &\underbrace{-\frac{3K_zK_\alpha}{L_S}\sin\left(\frac{\gamma}{2}\right)\cos\left(\frac{\gamma}{2}\right)\frac{\omega_e\omega}{\omega^2+\omega_e^2}}_{F_{z,a}} \end{aligned} \tag{13}$$

The first term corresponds to the conventional electrodynamic restoring force, although slightly diminished due to the angular misalignment γ. This force varies linearly with the axial position z and is thus entirely characterised by the underlying stiffness $k_{z,S}$. As illustrated in Fig. 2, it increases with the speed ω, regardless of the direction of rotation, eventually approaching an asymptotic value. In contrast, the second force term, $F_{z,a}$, arises from the angular misalignment between the upper and lower windings. It is independent from the rotor position z and therefore does not contribute to the machine axial stabilisation. As depicted in Fig. 2, its magnitude increases with the rotational speed ω until it reaches a peak value at the speed ω_e corresponding to the winding electrical pole and then declines asymptotically to zero. It should finally be noted that the direction of this force is directly determined by the rotor direction of rotation. Hence, this force can be advantageous for partially compensating speed-dependent axial load in applications consistently rotating in a fixed direction while limiting the increase of rotor axial displacement z. Otherwise, it acts as a disturbance that has to be counteracted by the first force term, thereby leading to additional losses.

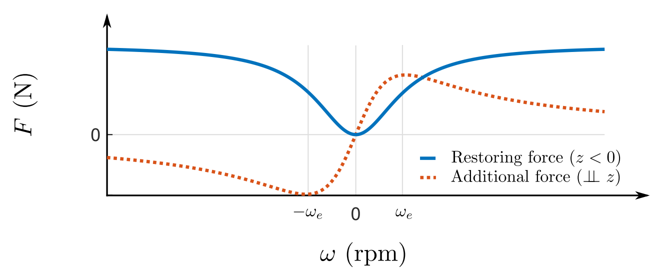

Fig. 2: Evolution of the restoring and additional force components with the rotational speed ω in quasi-static conditions.

3) Drag Torque: The torque $T_{\alpha,S}$ produced by the suspension current in quasi-static conditions can be determined by inserting (12) into (11):

$$\begin{aligned} T_{\alpha,S} = &-\left[\left(zK_z\cos\left(\frac{\gamma}{2}\right)\right)^2+\left(K_\alpha\sin\left(\frac{\gamma}{2}\right)\right)^2\right] \\ &\times\frac{3p}{L_s}\frac{\omega_e\omega}{\omega^2+\omega_e^2} \end{aligned} \tag{14}$$

As expected, it opposes to the self-bearing machine rotation and therefore corresponds to a drag torque. Its magnitude rises with the rotational speed ω up to the speed ω_e related to the electrical pole and then gradually decreases to zero. The angular misalignment γ introduces an additional term that

Parameter	Symbol	Unit	Value
Pole pair number	p	–	2
Flux constant	K_α	mWb	4.58
Flux gradient	K_z	Wb/m	0.84
Resistance	R	$m\Omega$	765
Suspension inductance	L_S	μH	56.5
External inductor resistance	R_{add}	$m\Omega$	64
External inductor inductance	L_{add}	μH	577.2
Angular misalignment	γ	degree	6.2

TABLE I: Global parameters of the prototype.

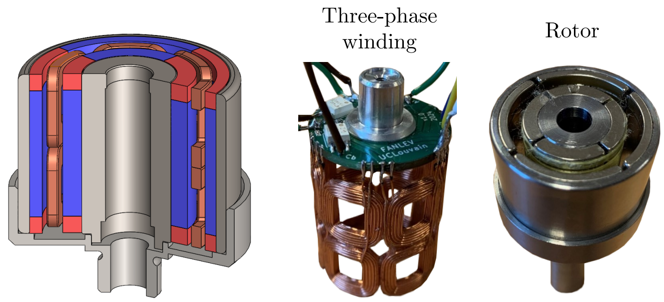

(a) (b)

Fig. 3: Prototype. (a) Structure. (b) Pictures.

does not evolve with the rotor axial displacement z, creating a disturbance even in centred position.

IV. Experimental Setup

This section describes the self-bearing machine prototype and the test stand developed for its characterisation and the validation of the extended electromechanical model.

A. Prototype

The prototype adopts a radial-flux structure, as represented in Fig. 3. The rotor includes internal and external permanent magnet arrangements, fixed on back irons, that generate a two pole-pair magnetic field while featuring a specific alternating magnetisation pattern in the axial direction to enhance the suspension performance [23]. The stator, placed between both magnet arrangements, consists of six upper and six lower concentrated coreless coils distributed among the three phases, corresponding to a slots-per-pole-per-phase (SPP) number of 1/2. External inductors are connected in series with the upper and lower windings of each phase to reduce the suspension electrical pole ω_e, thereby increasing the passive axial stiffness at low rotational speeds [25]. The global parameters of the self-bearing machine prototype, identified through the experimental methods described in [22], are summarised in Table I.

B. Test stand

The test stand is depicted in Fig. 4. A laser displacement sensor (Sick OD2-P30W04I0) allows to measure the rotor axial position z. An air bearing (New Way Air Bushing S301301) ensures the rotor radial and tilt guidance without

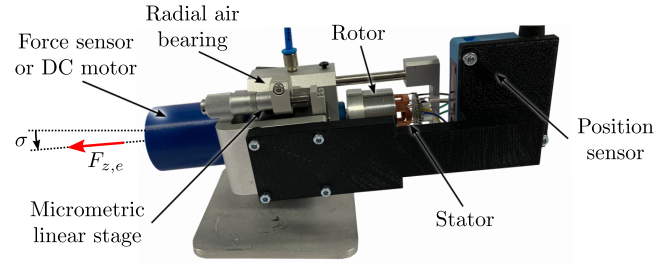

Fig. 4: Test stand.

impacting the axial dynamics. The prototype inclination σ with respect to the horizontal can be adjusted so as to apply a static axial load $F_{z,e} = mg\sin(\sigma)$ on the rotor, with m and g being the rotor mass and the gravitational acceleration. The test stand can be further instrumented in two configurations, enabling either the electromotive forces or the rotor axial behaviour during levitation to be investigated. In the first configuration, an external DC motor, mounted on a micrometric linear stage, is attached to the shaft to drive the rotor at constant rotational speed ω and fixed axial position z. In the second configuration, the self-bearing machine itself is driven through an off-the-shelf AC sensorless electronics (TI DRV8312-C2) developed for conventional electrical motors. The left axial landing bearing is fixed on a force sensor (Lorenz M-2416), thus allowing to measure the external force $F_{z,e}$ exerted on the rotor at standstill due to the prototype inclination σ.

V. Experimental Validation

This section aims to characterise the winding angular misalignment by analysing the electromotive forces and to validate the proposed electromechanical model through the evolution of the rotor axial position for different axial loads.

A. Electromotive Forces

The angular misalignment between the upper and lower windings results in a phase shift γ between the corresponding permanent magnet flux linkages, as expressed in (3). The latter can be identified through experimentation based on the analysis of the electromotive forces induced in the windings in open circuit, illustrated in Fig. 5, when the rotor is driven at constant rotational speed ω by the external DC motor which also fixes its axial position, yielding 6.2 electrical degrees.

B. Rotor Axial Position

The passive axial suspension force $F_{z,S}$ produced in quasi-static conditions by the machine, modelled in (13), is investigated by studying the evolution of the rotor displacement z with the rotational speed ω for different external forces $F_{z,e}$. To that end, the following methodology is adopted.

Firstly, an axial load $F_{z,e}$ is applied on the rotor by tilting the prototype and determined with the force sensor. The rotor is accelerated up to a rotational speed ω of 4500 (rpm). The driver is then disconnected from the three-phase winding, preventing the motor currents from flowing and thus generating any torque $T_{\alpha,M}$ and axial force $F_{z,M}$. Consequently, the

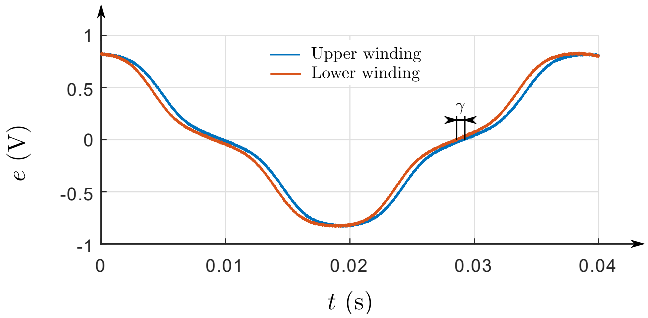

Fig. 5: Evolution with time of the electromotive forces induced in the upper and lower windings of phase A at a rotational speed ω of 775 (rpm) in centred position.

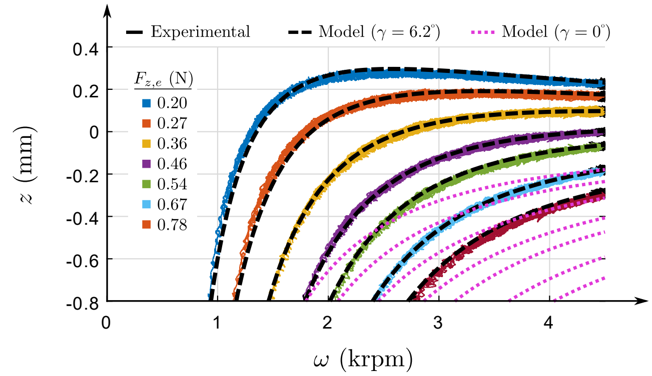

Fig. 6: Evolution of the axial position z with the rotational speed ω for different external force $F_{z,e}$.

axial dynamics solely results from the axial load $F_{z,e}$ and the passive axial force $F_{z,S}$. As the rotor decelerates due to the electrodynamic and aerodynamic drag torques, the time evolution of the axial position z and rotational speed ω is recorded until the shaft contacts the landing bearing, and both these experimental data are finally combined. It should be noted that, although neither the axial position z nor the rotational speed ω remain constant throughout this test, the measurements can be considered to reflect quasi-static conditions. Indeed, the electrical phenomena are much faster than the mechanical dynamics occurring during the rotor deceleration, allowing the suspension currents and the resulting forces to be assumed to evolve in steady state.

Fig. 6 illustrates the evolution of the rotor displacement z with the rotational speed ω for different axial loads $F_{z,e}$. The solid line represents the experimental data while the dashed and dotted lines correspond to the equilibrium position extracted from the electromechanical model in quasi-static conditions when accounting for the actual and zero winding angular misalignment γ respectively. The close agreement between the two former allows us to validate the proposed model whereas the significant discrepancy between both models highlights the substantial influence that this misalignment can have on the rotor axial suspension. Interestingly, this manufacturing imperfection leads the rotor to start levitating from a lower rotational speed ω and to get closer to the centred position, $z = 0$, than in the ideal case. Indeed, as discussed in Section III-D, the direction of the additional force $F_{z,a}$, that arises from the angular misalignment γ, directly depends on the rotor direction of rotation. The latter is selected so that this force opposes the external force $F_{z,e}$, partially compensating or even exceeding it depending on the considered case. This demonstrates the potential interest that this additional force could have in applications rotating in a unique direction.

VI. Conclusion

This paper analyses the effect of an angular misalignment between the upper and lower windings, caused by manufacturing imperfections, on the force and torque capabilities of passively levitated self-bearing machines.

The electromechanical model that predicts their axial and rotational rotor dynamics is adapted to account for this non-ideality, revealing that the conventional passive restoring force is slightly reduced, on the one hand, and that two additional force terms are generated, on the other hand. The first term is produced by the quadrature-axis motor current, that is responsible for the torque production, and acts as an axial disturbance on the system. The second one results from the passively induced suspension current and therefore evolves with the rotational speed. It is independent from the rotor axial displacement and its direction is determined by the rotor direction of rotation. Applications involving unidirectional rotation could thus benefit from this additional force to partially offset an external axial load, thereby minimising the rotor axial displacement. Regarding the rotational dynamics, the angular misalignment between the upper and lower windings introduces two additional torque components. The former arises from the direct-axis motor current and can be considered negligible whereas the latter is created by the suspension currents regardless of the rotor axial displacement, resulting in additional losses even in centred position.

Finally, an experimental study is performed based on a prototype and a dedicated test stand, validating the passive suspension forces, retrieved from the electromechanical model under quasi-static conditions, and underlining the importance of considering this non-ideality of the armature winding.

References

[1] T. Pei, D. Li, J. Liu, J. Li, and W. Kong, "Review of bearingless synchronous motors: Principle and topology," *IEEE Transactions on Transportation Electrification*, vol. 8, no. 3, pp. 3489–3502, 2022.

[2] W. Gruber, W. Bauer, D. Wetsch, B. Klammer, and N. Kurita, "Implementation of a bearingless axial-force/torque motor fan with flex-pcb windings," in *2019 IEEE International Electric Machines Drives Conference (IEMDC)*, May 2019, pp. 179–184.

[3] J. Asama, D. Kanehara, T. Oiwa, and A. Chiba, "Development of a compact centrifugal pump with a two-axis actively positioned consequent-pole bearingless motor," *IEEE Transactions on Industry Applications*, vol. 50, no. 1, pp. 288–295, Jan 2014.

[4] H. Onuma, T. Masuzawa, and M. Murakami, "Development of a small magnetic levitated centrifugal blood pump using a radial type self-bearing motor and axial position change of rotor-impeller by rotational magnetic field," *Mechanical Engineering Journal*, vol. 4, no. 5, pp. 17–00 066–17–00 066, 2017.

[5] P. Puentener, M. Schuck, J. W. Kolar, and D. Steinert, "Comparison of bearingless slice motor topologies for pump applications," in *2019 IEEE International Electric Machines Drives Conference (IEMDC)*, May 2019, pp. 9–16.

[6] J. Chen, J. Zhu, and E. L. Severson, "Review of bearingless motor technology for significant power applications," *IEEE Transactions on Industry Applications*, vol. 56, no. 2, pp. 1377–1388, 2020.

[7] J. Abrahamsson, J. Ogren, and M. Hedlund, "A fully levitated cone-shaped lorentz-type self-bearing machine with skewed windings," *IEEE Transactions on Magnetics*, vol. 50, no. 9, pp. 1–9, 2014.

[8] W. Li, K. T. Chau, T. W. Ching, Y. Wang, and M. Chen, "Design of a high-speed superconducting bearingless machine for flywheel energy storage systems," *IEEE Transactions on Applied Superconductivity*, vol. 25, no. 3, pp. 1–4, June 2015.

[9] Y. Yuan, Y. Sun, and Y. Huang, "Design and analysis of bearingless flywheel motor specially for flywheel energy storage," *Electronics Letters*, vol. 52, no. 1, pp. 66–68, 2016.

[10] A. Tuysuz, T. Achtnich, C. Zwyssig, and J. Kolar, "A 300 000-r/min magnetically levitated reaction wheel demonstrator," *IEEE Transactions on Industrial Electronics*, vol. 66, no. 8, pp. 6404–6407, Aug. 2019.

[11] K. Raggl, T. Nussbaumer, and J. W. Kolar, "A comparison of separated and combined winding concepts for bearingless centrifugal pumps," *Journal of power electronics*, vol. 9, no. 2, pp. 243–258, 2009.

[12] D. Dietz and A. Binder, "Comparison between a bearingless pm motor with separated and combined winding for torque and lateral force generation," in *2019 21st European Conference on Power Electronics and Applications (EPE '19 ECCE Europe)*, 2019, pp. P.1–P.10.

[13] A. Khamitov, N. P. Petersen, and E. L. Severson, "Combined windings for bearingless motors - an overview," in *2023 IEEE Energy Conversion Congress and Exposition (ECCE)*, 2023, pp. 4628–4635.

[14] M. Osa, T. Masuzawa, T. Saito, and E. Tatsumi, "Magnetic levitation performance of miniaturized magnetically levitated motor with 5-dof active control," *Mechanical Engineering Journal*, vol. 4, no. 5, pp. 17–00 007, 2017.

[15] M. Osa, T. Masuzawa, K. Yamaguchi, and E. Tatsumi, "Double stator axial gap type ultra-compact 5-dof controlled self-bearing motor for rotary pediatric ventricular assist device," *IEEE Transactions on Industry Applications*, vol. 57, no. 6, pp. 6744–6753, 2021.

[16] H. Mitterhofer, B. Mrak, and W. Gruber, "Comparison of high-speed bearingless drive topologies with combined windings," *IEEE Transactions on Industry Applications*, vol. 51, no. 3, pp. 2116–2122, May 2015.

[17] B. S. Weinreb, M. Noh, D. C. Fyler, and D. L. Trumper, "Design and implementation of a novel interior permanent magnet bearingless slice motor," *IEEE Transactions on Industry Applications*, vol. 57, no. 6, pp. 6774–6782, 2021.

[18] K. Kant and D. L. Trumper, "Motor castellation for enhancing the passive stiffness of bearingless slice motors," *IEEE Transactions on Energy Conversion*, vol. 40, no. 1, pp. 615–622, 2025.

[19] W. Bauer and W. Amrhein, "Electrical design considerations for a bearingless axial-force/torque motor," *IEEE Transactions on Industry Applications*, vol. 50, no. 4, pp. 2512–2522, July 2014.

[20] J. Asama, T. Tai, and A. Chiba, "Development of axial-flux single-drive bearingless motor with one-axis active positioning," *IEEE Transactions on Industry Applications*, vol. 57, no. 6, pp. 6792–6800, 2021.

[21] H. Sugimoto and A. Chiba, "Dynamic modeling and experimental validations of passing through critical speeds by high acceleration in one-axis actively positioned bearingless motors," *IEEE Transactions on Industry Applications*, vol. 57, no. 6, pp. 6956–6964, 2021.

[22] J. Van Verdeghem, M. Lefebvre, V. Kluyskens, and B. Dehez, "Dynamical modeling of passively levitated electrodynamic thrust self-bearing machines," *IEEE Transactions on Industry Applications*, vol. 55, no. 2, pp. 1447–1460, March 2019.

[23] G. C. Rubio, Y. Fujii, and A. Chiba, "A bearingless motor with passive electrodynamic suspension in axial direction," *IEEE Transactions on Industry Applications*, vol. 57, no. 6, pp. 6812–6822, 2021.

[24] J. Van Verdeghem, A. Robert, S. Herrman, and B. Dehez, "Impact of ferromagnetic yokes on axial flux passively levitated self-bearing machines," in *2022 25th International Conference on Electrical Machines and Systems (ICEMS)*, 2022, pp. 1–6.

[25] J. Van Verdeghem, V. Kluyskens, and B. Dehez, "Experimental investigations on passively levitated electrodynamic thrust self-bearing motors," *IEEE Transaction on Industry Applications*, vol. 55, no. 5, pp. 4743–4753, Sep. 2019.

[26] J. Van Verdeghem and B. Dehez, "Fully passively levitated self-bearing machine implemented within a reaction wheel," *IEEE Trans. on Ind. App.*, vol. 57, no. 6, pp. 5782–5795, 2021.

[27] G. C. Rubio, Y. Fujii, and A. Chiba, "Requirements for full passive suspension on a bearingless motor with electrodynamic axial stabilization and radial permanent magnet bearings," in *2021 IEEE Energy Conversion Congress and Exposition (ECCE)*, 2021, pp. 3936–3942.

[28] G. C. Rubio, V. C. Hothur Komal, Y. Fujii, and A. Chiba, "Experimental verification of passive axial electrodynamic suspension in a bearingless motor," *IEEE Open Journal of Industry Applications*, pp. 1–12, 2023.

[29] V. C. H. Komal, Y. Fujii, and A. Chiba, "Axial electrodynamic suspension in a hybrid bearingless motor with active and passive axial stabilization," *Journal of the Japan Society of Applied Electromagnetics and Mechanics*, vol. 32, no. 2, pp. 331–338, 2024.

[30] J. Van Verdeghem, E. Severson, and B. Dehez, "Hybrid active-passive actuation approach of passively levitated thrust self-bearing machines," *IEEE Transactions on Industry Applications*, vol. 57, no. 6, pp. 7035–7045, 2021.